Supplementary Materials for

Scalable and Sustainable Manufacturing of Intermetallic Nanocrystals for Economical Water Splitting

Mingjin Cui,‡* Haijiao Liu,‡ Ke Chen,‡ Xinwei Shi, Bo Xu, Chenlu Jiang, Dehui Li, Ding Yuan, Yuhai Dou, Chao Wu, Menghao Yang,* Shixue Dou, Yu Ding*

Corresponding author: Mingjin Cui, mjcui@usst.edu.cn; Menghao Yang, menghaoyoung@tongji.edu.cn; Yu Ding, yuding@nju.edu.cn

This PDF file includes:

Figs. S1 to S19

Table S1 to S15

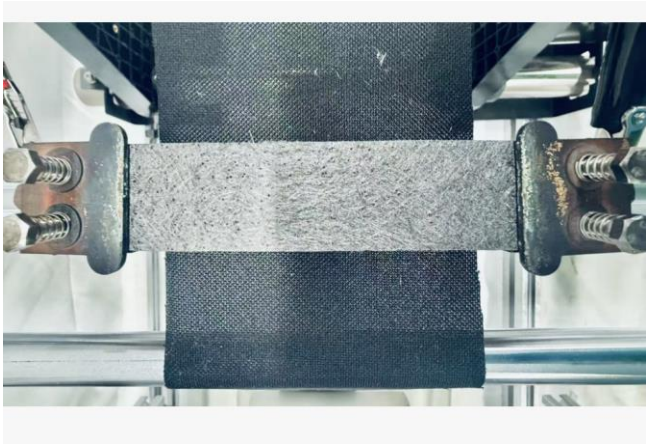

Fig. S1 Top-view photograph of the integrated radiative heating zone before heating

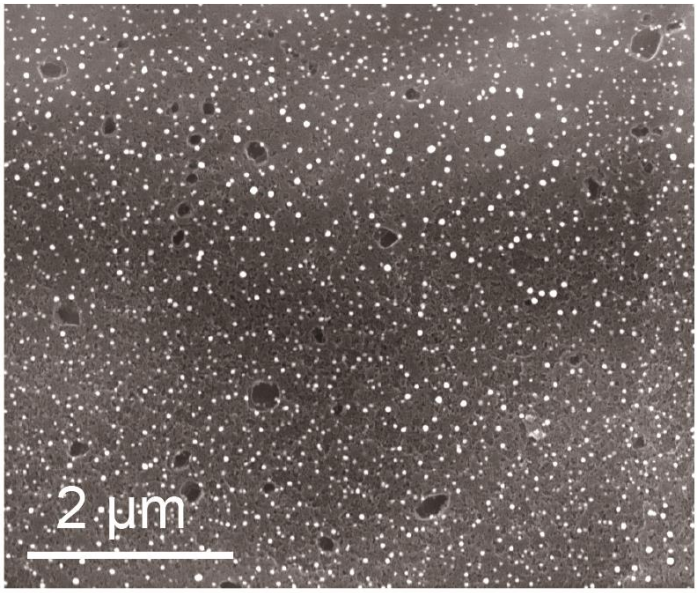

Fig. S2 Low-magnification SEM image of $L1_2$-Ni_3Fe iNCs. The scale bar represents 2 µm, and indicative of uniform atomic dispersion of $L1_2$-Ni_3Fe iNCs across the substrate.

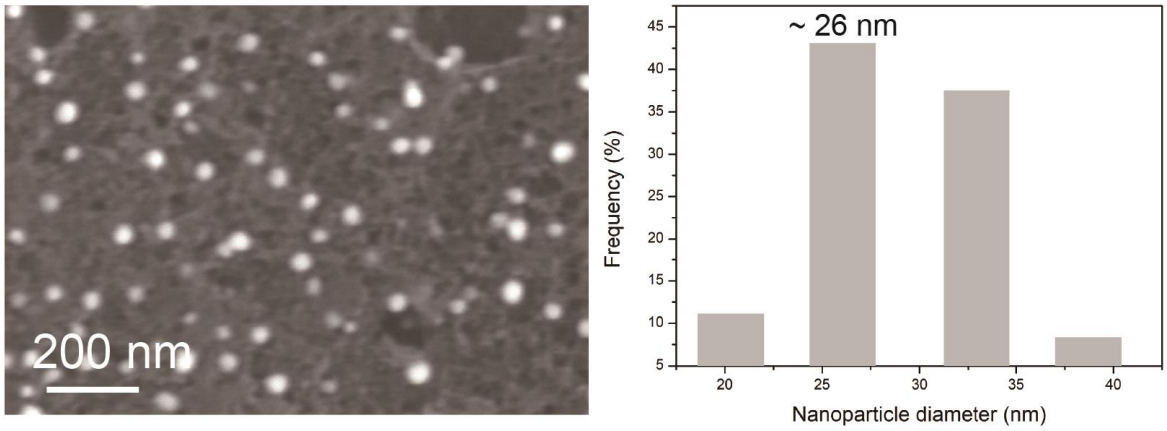

Fig. S3 High-magnification SEM image of $L1_2$-Ni_3Fe iNCs. The left showing uniform nanoparticle dispersion and a corresponding particle size distribution histogram on the right with an average diameter of approximately 26 nm.

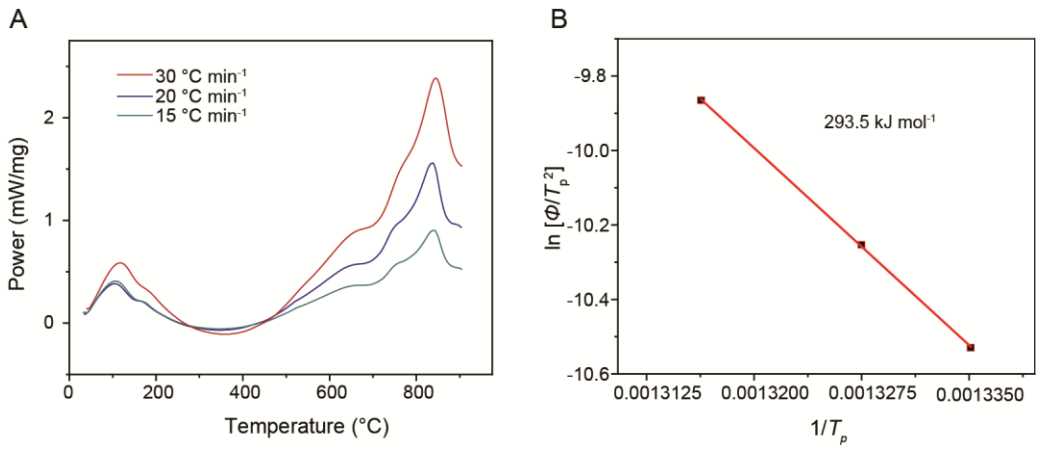

Fig. S4 Structural characterizations of Ni_3Fe. (**A**) Differential scanning calorimetry (DSC) profiles of Ni_3Fe recorded at multiple linear heating rates (15, 20, and 30 K min^{-1}), illustrating the progressive shift of the endothermic/exothermic peak positions with increasing rate. Panel (**B**) plots $\ln(\Phi/T_p^2)$ versus $1/T_p$ (Kissinger analysis) to extract the apparent activation energy (E_a) for the Ni_3Fe phase transformation, yielding a value of 293.5 kJ mol^{-1}. All measurements were conducted under a constant N_2 flow of 50 mL min^{-1}.

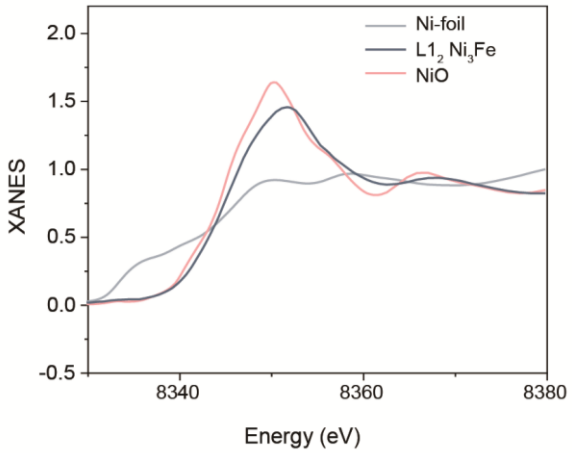

Fig. S5 Ni K-edge X-ray absorption spectroscopy characterization of the $L1_2$-Ni_3Fe as well as the reference Ni foil and NiO samples. XANES spectra, highlighting the edge-position shift and white-line intensity differences: $L1_2$-Ni_3Fe exhibits a modest positive shift relative to Ni foil, indicative of partial electron withdrawal, and a suppressed white-line compared to NiO, consistent with its metallic bonding character.

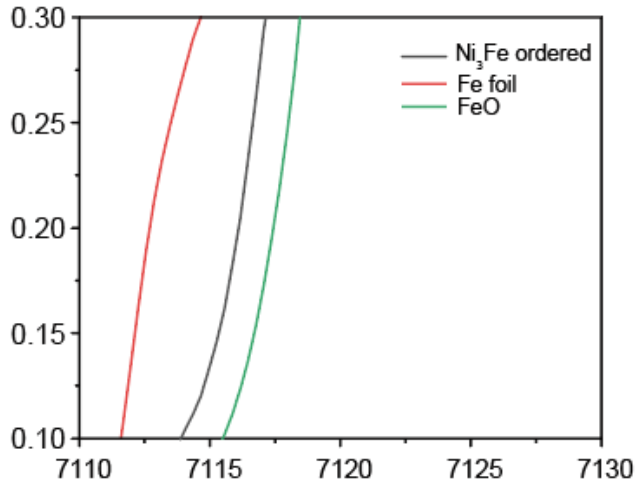

Fig. S6 Fe K-edge XANES spectra of $L1_2$-Ni_3Fe intermetallic nanocrystals (red), Fe foil (black) and FeO (blue). The lower panel shows a zoomed view of the 1s→3d pre-edge region (7110-7114 eV). The main absorption edge of $L1_2$-Ni_3Fe (≈7120 eV) coincides with metallic Fe foil, indicating predominantly Fe^0, whereas the FeO edge is shifted ≈1.5 eV higher, characteristic of Fe^{2+}. In the magnified pre-edge region, $L1_2$-Ni_3Fe exhibits a slightly enhanced peak intensity relative to Fe foil, signifying increased 3d vacancies and altered local symmetry in the ordered intermetallic lattice.

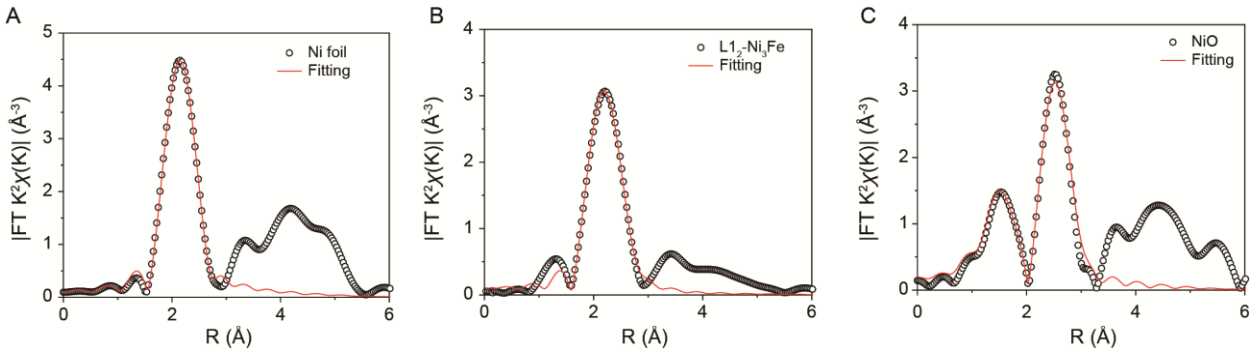

Fig. S7 Extended X-ray absorption fine structure and FT-XAFS fitting data for the Ni foil (**A**), $L1_2$-Ni_3Fe (**B**), and NiO (**C**) at Ni *K*-edge.

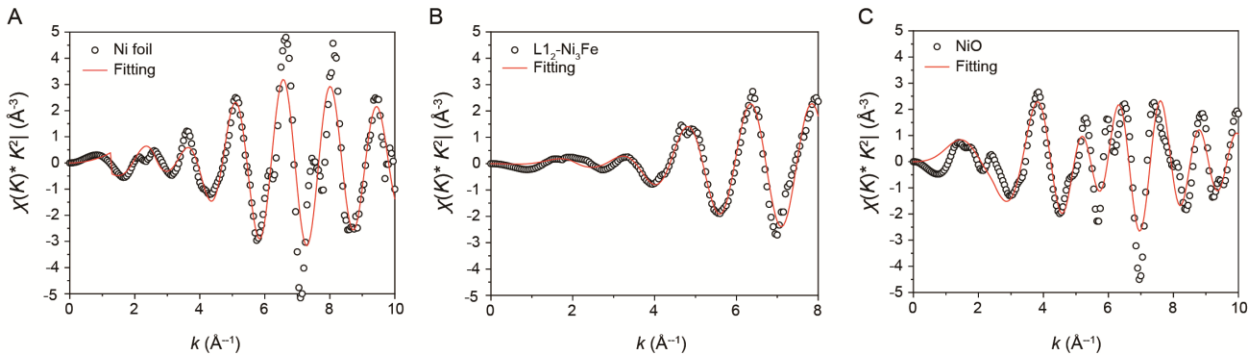

Fig. S8 Inverse FT-EXAFS fitting for the Ni foil, $L1_2$-Ni_3Fe, and NiO at Ni *K*-edge.

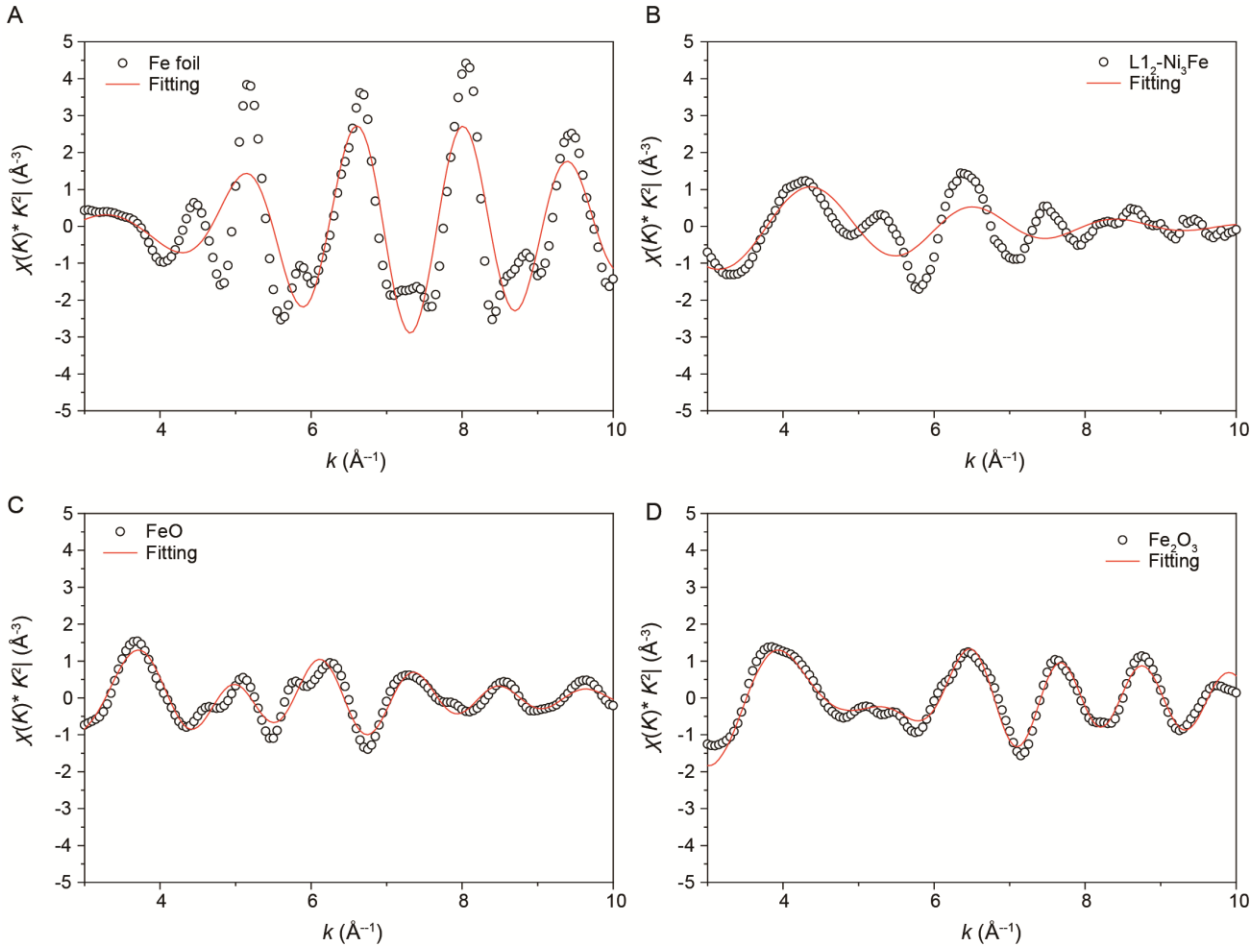

Fig. S9 Inverse FT-EXAFS fitting for the Fe foil, $L1_2$-Ni_3Fe, FeO, and Fe_2O_3 at Fe *K*-edge.

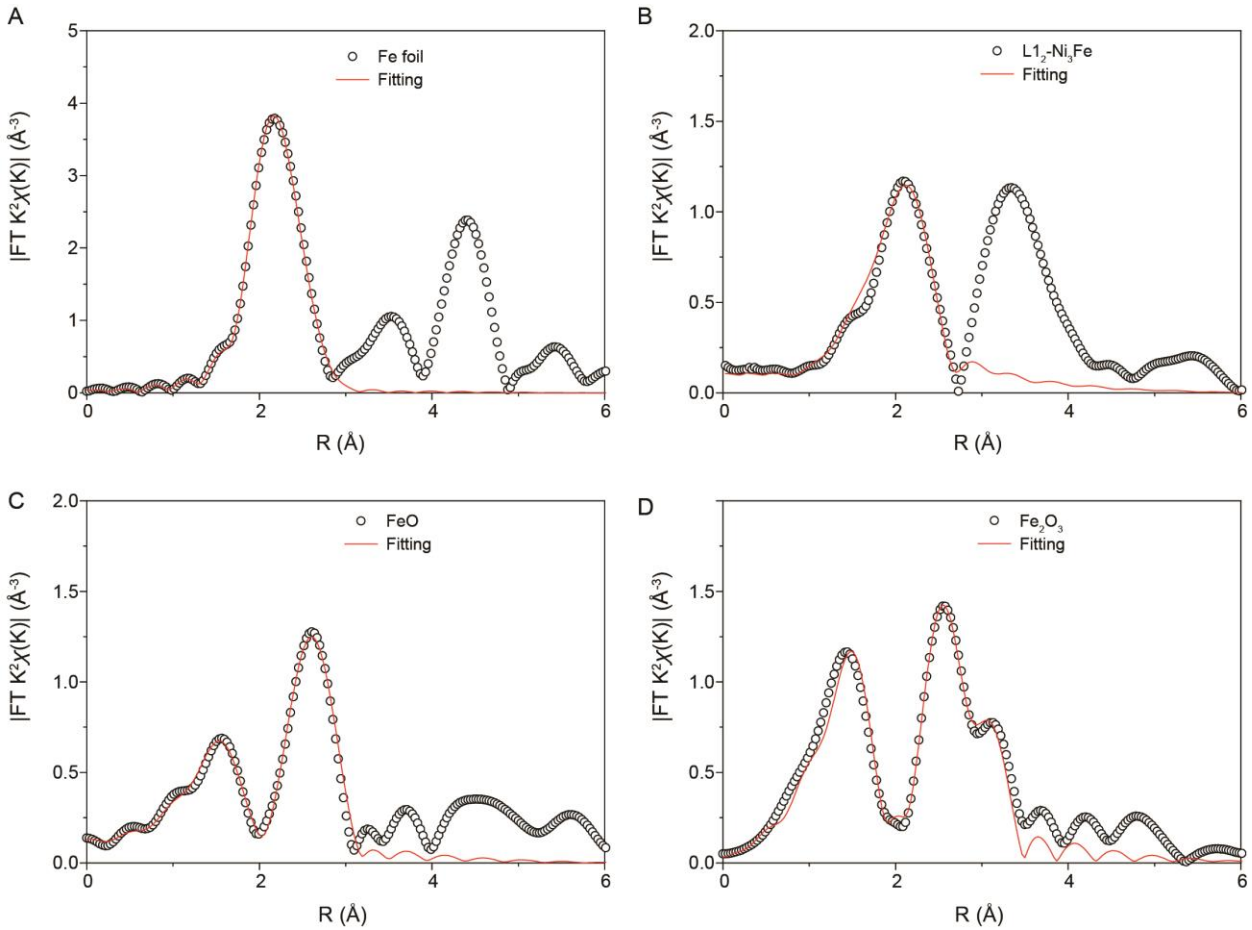

Fig. S10 Extended X-ray absorption fine structure (EXAFS) and FT-XAFS fitting data of the Fe foil, $L1_2$-Ni_3Fe, FeO, and Fe_2O_3 at Fe *K*-edge.

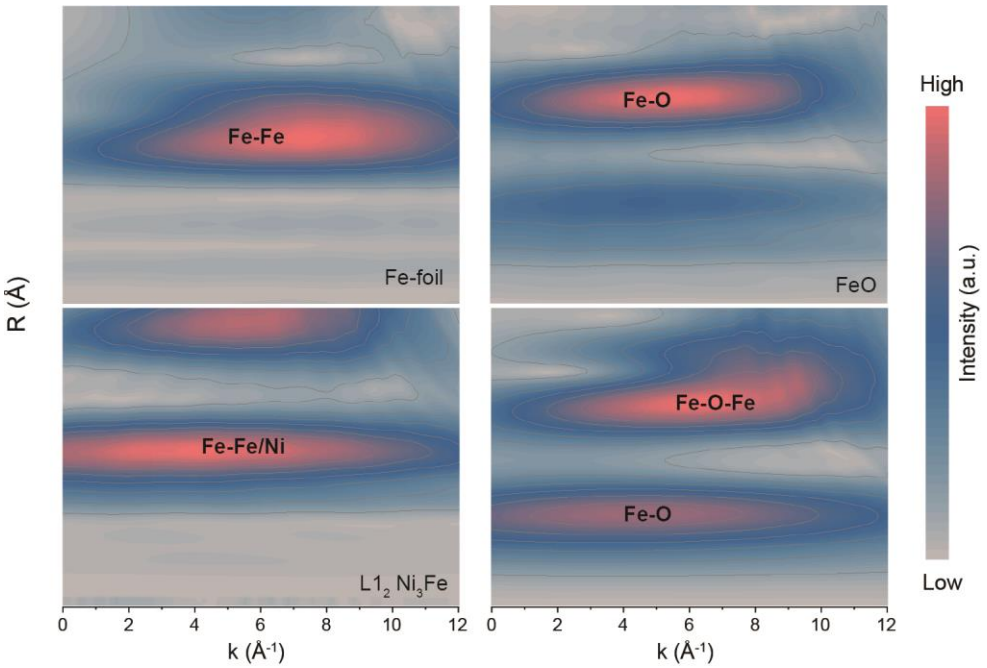

Fig. S11 WT EXAFS spectra for the Fe foil, $L1_2$-Ni_3Fe, FeO, and Fe_2O_3 at Fe *K*-edge.

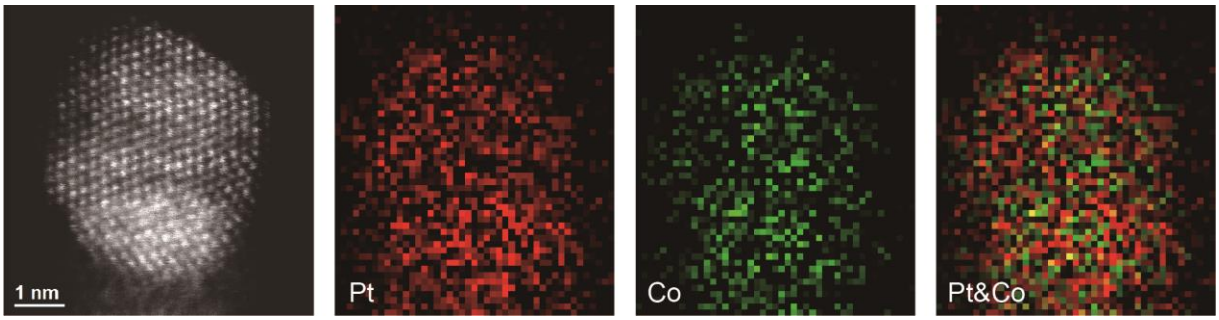

Fig. S12 (a) HAADF-STEM image of a Pt_3Co nanoparticle, where the atomic-scale Z-contrast between Pt (bright) and Co (dark) confirms a chemically $L1_2$ ordered structure. (b) Corresponding EDS elemental maps for Pt and Co, showing a homogeneous distribution without segregation. The successful application to $L1_2$-Pt_3Co, underscores the versatility of this synthesis approach.

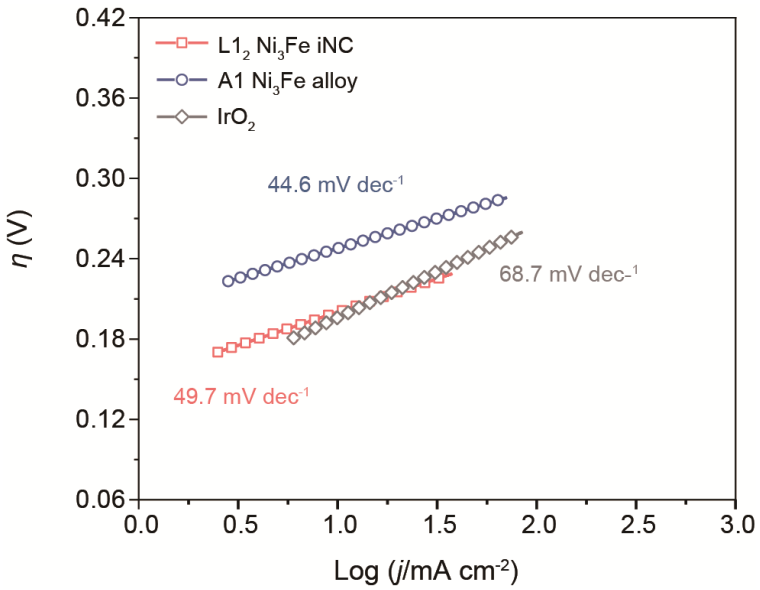

Fig. S13 Tafel plots derived from LSV curves for $L1_2$-Ni_3Fe iNC (red squares), A1 Ni_3Fe alloy (blue circles), and commercial IrO_2 (gray diamonds) in alkaline electrolyte. The corresponding Tafel slopes are 49.7, 44.6, and 68.7 mV dec^{-1}, respectively, indicating faster HER kinetics for the $L1_2$-Ni_3Fe iNC and A1 Ni_3Fe alloy compared with IrO_2. The lower Tafel slope reflects more favorable Volmer-Heyrovsky or Volmer-Tafel pathways, highlighting the enhanced intrinsic activity conferred by the ordered intermetallic and alloy structures.

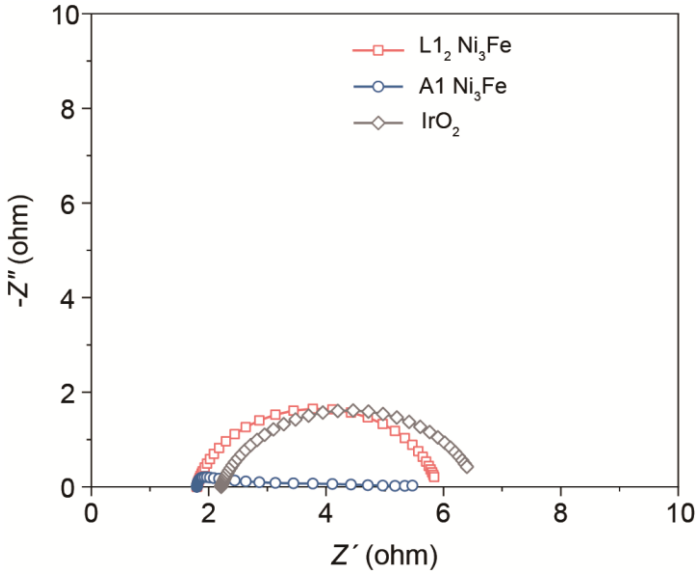

Fig. S14 Electrochemical impedance spectroscopy Nyquist plots of $L1_2$-Ni_3Fe, A1 Ni_3Fe, and commercial IrO_2.

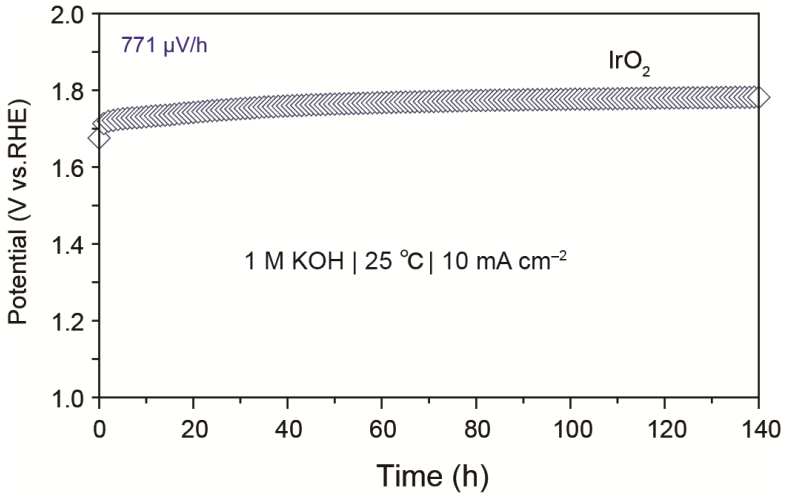

Fig. S15 Chronopotentiometry curves of commercial IrO_2 recorded at a constant current density of 10 mA cm^{-2} in 1.0 M KOH, showing the potential increase over 140 h of continuous operation corresponding to a degradation rate of 771 μV h^{-1}.

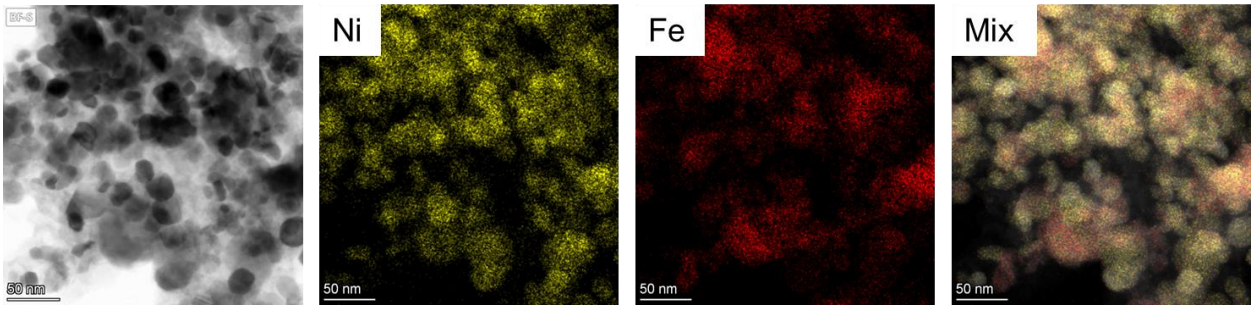

Fig. S16 Post-mortem TEM images of the used catalyst show that the nanoparticles retain their original size (~20-30 nm) and morphology without any sign of agglomeration. EDS mapping confirms that the homogeneous elemental distribution is preserved.

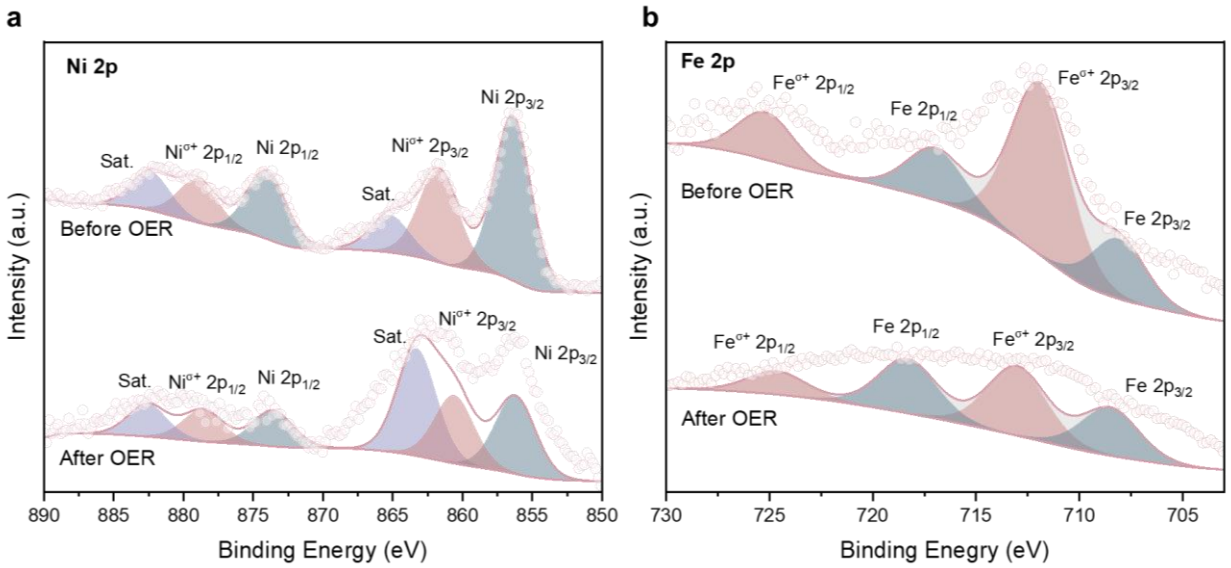

Fig. S17 XPS analysis indicates that the Ni 2p core-level XPS spectra of the $L1_2$-Ni_3Fe iNCs display characteristic features of both metallic and oxidized Ni species. The high-resolution Ni $2p_{3/2}$ spectrum shows peaks at 856.38, 861.66, and 865.18 eV, while the Ni $2p_{1/2}$ region contains peaks at 874.00, 878.94, and 882.32 eV. The dominant peaks at 856.38 and 874.00 eV correspond to metallic Ni, confirming that Ni remains predominantly in the metallic state. The peaks at 861.66 and 878.94 eV arise from oxidized Ni species, likely originating from unavoidable surface oxidation , whereas the features at 865.18 and 882.32 eV are assigned to satellite peaks. The Fe 2p spectra further reveal two chemical states, including metallic Fe (708.08 and 716.96 eV) and $Fe^{\delta+}$ (711.88 and 725.18 eV). Compared with the pristine sample, the used catalyst after OER testing exhibits diminished metallic Ni and Fe signals (Ni^0 and Fe^0) in the Ni $2p_{3/2}$ and Fe $2p_{3/2}$ regions, accompanied by increased intensities of Ni(II/III) and their associated satellite features. These changes indicate surface oxidation of the $L1_2$-Ni_3Fe iNCs during OER, consistent with the intrinsically unavoidable oxidation of Ni-Fe surfaces under electrochemical OER conditions.

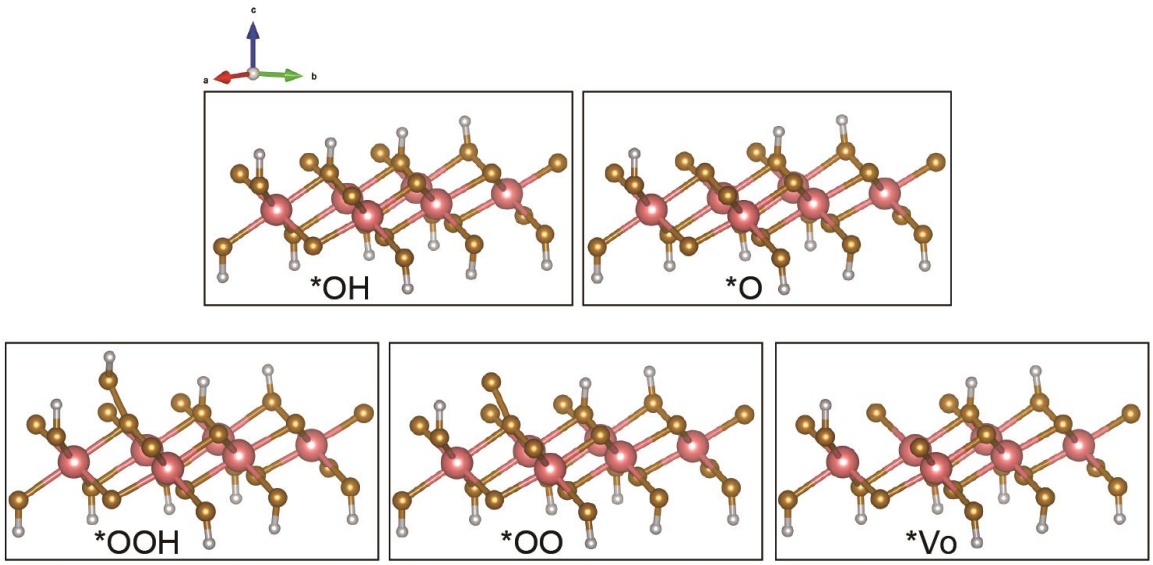

Fig. S18 Three-dimensional adsorption models of the lattice oxygen-mediated pathway on NiOOH, showing *OH adsorption, *O formation, *OOH coupling, and O_2 desorption (Fe: blue; Ni: red; O: orange; H: white).

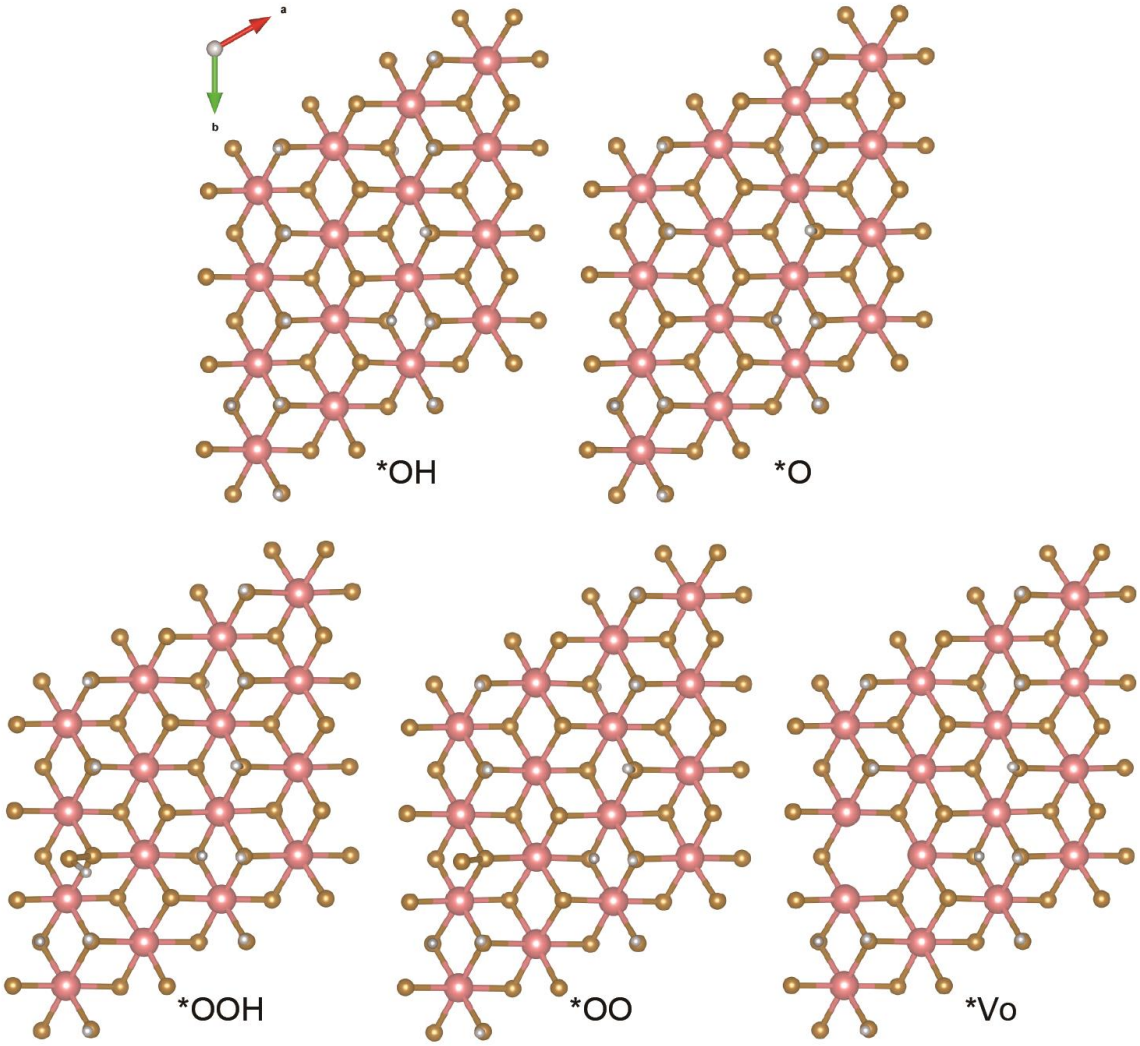

Fig. S19 Adsorption models of the LOM pathway on NiOOH. Shown are (i) initial *OH adsorption at the Fe active site, (ii) formation of the *O intermediate via deprotonation, (iii) lattice oxygen involvement in O-O coupling to form *OOH, and (iv) desorption of molecular O_2, with all slab models viewed along the [001] direction and metal atoms color-coded for clarity (Fe: blue; Ni: red; O: orange; H: white).

Table S1 The comparison of productivity and preparation time between the traditional synthesis process with our roll-flow system synthesis

Catalysts	Synthesis time	Productivity (g/min)	Method	Temperature	Waste	Sustained working time	References
Ni_3Fe	1 min	10 g/min	Roll-flow heating	650 °C	/	1 min/cycle	This work
Ni_3Fe	~10 h	/	Wet chemistry	450 °C	DMF	/	Small 2024, 2407116
Ni_3Fe	~7 days	/	Pyrolysis	120 °C	Tetrahydrofuran and dichloromethane	/	Nano Research, 2023, 16(5), 6710-6720
FeMnPt	~5 h	/	Annealing	780 °C	NaCl	/	ACS Appl. Nano Mater. 2024, 7, 8093−8101
PtPbBi	~2.5 h	/	Co-reduction	220 °C		/	Angew. Chem. Int. Ed. 2024, 63, e202405173
FeCoNiCuPd	~36 h	/	Wet chemistry	60 °C	pyridine	/	Adv. Mater. 2022, 34, 2110128
PtNiGa	2.5 h	/	Wet chemistry	160 °C	cetyltrimethylammonium bromide	/	Chin. Chem. Lett. 2024. 35. 108445
$(Pt_{0.9}Rh_{0.1})_3V$	7 h	/	Annealing	800 °C	/	/	Angew. Chem. Int. Ed. 2024, e202402496
(Fe, Co, Ni)/Pt	~13 h	/	Microwave-assisted polyol reduction	190 °C	phosphide	/	Adv. Mater. 2023, 35, 2207995

PtFeIr	2 h	/	Annealing	690 °C	oleylamine	/	Angew. Chem. Int. Ed. 2022, 61, e202113278
PtZnCu	16 h	/	Ball milling and annealing	750 °C	dimethylimidazole	/	ACS Appl. Energy Mater. 2022, 5, 12219 −12226
$(FeCoNi)_2TiSb$	20 h	/	Ball milling and spark plasma sintering	800 °C	/	/	Intermetallics 171 (2024) 108343
Pd_3Pb@PdBi	2 h	/	Wet-Chemical Epitaxial Growth	220 °C	oleylamine	/	Adv. Funct. Mater. 2024, 2403023
PtCu	3 h	/	Annealing	500 °C	/	/	Small Struct. 2024, 5, 2300537
PtPdFeCoNi	10 h	/	Annealing	480 °C	/	/	Adv. Energy Mater. 2024, 14, 2303923
Pt_4FeCoCuNi	2 h	/	Annealing	1000 °C	2,2′-bithiophene	/	Adv. Mater. 2023, 35, 2302067
PtRhFeNiCu	2 h	/	Annealing	700 °C	/	/	SmartMat. 2023;4:e1117

Table S2 A list of chemicals used in the synthesis of samples.

Regent	Price	Source
$FeCl_3·6H_2O$ CAS:10025-77-1	$298 /1000g	https://www.sigmaaldrich.cn/CN/zh/search/10025-77-1?focus=products&page=1&perpage=30&sort=relevance&term=10025-77-1&type=cas_number Access time: Jul. 18, 2025
$NiCl_2·6H_2O$ CAS:7791-20-0	$565/1000g	https://www.sigmaaldrich.cn/CN/zh/search/7791-20-0?focus=products&page=1&perpage=30&sort=relevance&term=7791-20-0&type=cas_number Access time: Jul. 18, 2025
Ketjenblack ECP600JD	$27.8/50g	SUZHOU SINERO TECHNOLOGY CO.,LTD Access time: Apr. 20, 2024
$FeSO_4·7H_2O$ CAS: 7782-63-0	$251/1000g	https://www.sigmaaldrich.cn/CN/zh/search/7782-63-0?focus=products&page=1&perpage=30&sort=relevance&term=7782-63-0&type=cas_number Access time: Jul. 18, 2025
$Ni(NO_3)_2·6H_2O$ CAS: 13478-00-7	$108/100g	https://www.sigmaaldrich.cn/CN/zh/search/13478-00-7?focus=products&page=1&perpage=30&sort=relevance&term=13478-00-7&type=cas_number Access time: Jul. 18, 2025
$(CH_3)_2CHOH$ CAS: 67-63-0	$17.3/1L	https://www.sigmaaldrich.cn/CN/zh/search/67-63-0?focus=products&page=1&perpage=30&sort=relevance&term=67-63-0&type=cas_number Access time: Jul. 18, 2025
GO ($C_xO_yH_z$)	$300/1g	https://www.sigmaaldrich.cn/CN/zh/search/cxoyhz?focus=products&page=1&perpage=30&sort=relevance&term=$C_xO_yH_z$&type=product Access time: Jul. 18, 2025
$Ni(acac)_2$ CAS: 3264-82-2	$399/50g	https://www.sigmaaldrich.cn/CN/zh/search/3264-82-2?focus=products&page=1&perpage=30&sort=relevance&term=3264-82-2&type=cas_number Access time: Jul. 18, 2025
$Fe(acac)_3$ CAS: 14024-18-1	$355/500g	https://www.sigmaaldrich.cn/CN/zh/search/14024-18-1?focus=products&page=1&perpage=30&sort=relevance&term=14024-18-1&type=cas_number Access time: Jul. 18, 2025
NF (20×20 cm)	$14.3/copy	SCI Materials Hub https://www.scimaterials.cn Access time: May. 10, 2024
KBr CAS: 7758-02-3	$128.7/100g	https://www.sigmaaldrich.cn/CN/zh/search/7758-02-3?focus=products&page=1&perpage=30&sort=relevance&term=7758-02-3&type=cas_number Access time: Jul. 18, 2025
CH_3CH_2OH CAS: 64-17-5	$45.4/1L	https://www.sigmaaldrich.cn/CN/zh/search/64-17-5?focus=products&page=1&perpage=30&sort=relevance&term=64-17-5&type=cas_number Access time: Jul. 18, 2025

Table S3 Life-cycle impact of climate change.

Scenario	**This work**	**Ref.1**	**Ref.2**	**Ref.3**
Water deionised	7.66E-6	0.001249	0.000156083	0
Carbon	1.13E-5	0	0	0
Nickel	0.000168	5.1993	2.60E-05	0.00027851
Iron(III)chloride	1.21E-5	0	2.85E-06	3.60E-5
Iron sulfate	0	0.002578	0	0
Potassium hydrooxide	0	0	0	0.001049708
Argon	0.0027	0	0.013490966	0
Melamine	8.79E-5	0	0	0
Isopropanol	0	4.1954	0	0
Bromine	0	0	0	0.0030969
Ethanol	0	0	0	0.0076769
Sulfuric acid	0	0	0.001605481	0
Graphite	0	0	2.96E-06	0
Hydrogen peroxide	0	0	6.29E-9	0
Potassium permanganate	0	0	0.000179573	0
Glucose	0	0	0	0.00196078
Chlorine	1.26E-5	0	2E-6	0
Electricity	0.402315	1.143	1.1244153	1.1242638
Sum	0.43	10.541527	1.14	1.1383625

Unit: kg CO_2 eq.

Table S4 Life-cycle impact of water depletion.

Scenario	This work	Ref.1	Ref.2	Ref.3
Water deionised	5.05E-6	0.000823	0.000103	0
Carbon	2.81E-8	0	0	0
Nickel	2.05E-6	0.059425	3.17E-07	3.39E-6
Iron(III)chloride	2.41E-7	0	5.68E-08	7.17E-7
Iron sulfate	0	1.68E-5	0	0
Potassium hydrooxide	0	0	0	9.29E-6
Argon	0.000719	0	0.000359615	0
Melamine	4.36E-6	0	0	0
Isopropanol	0	0.030774	0	0
Bromine	0	0	0	1.35E-5
Ethanol	0	0	0	0.0020195
Sulfuric acid	0	0	1.79E-06	0
Graphite	0	0	1.48E-08	0
Hydrogen peroxide	0	0	2.48E-06	0
Potassium permanganate	0	0	1.78E-06	0
Glucose	0	0	0	6.01E-5
Chlorine	4.37E-7	0	6.93E-8	0
Electricity	0.0139	0.039629	0.0390	0.0389796
Sum	0.0147	0.13067	0.0395	0.0411

Unit: m^3

Table S5 Life-cycle impact of human carcinogenic and non-carcinogenic toxicity.

Scenario	**This work**	**Ref.1**	**Ref.2**	**Ref.3**
Water deionised	6.56E-6	0.00107	1.95E-8	0
Carbon	5.51E-6	0	0	0
Nickel	0.0029	110.5198	0.000450	1.87E-5
Iron(III)chloride	1.21E-5	0	7.257E-6	9.174E-5
Iron sulfate	3.09E-6	0.00793	0	0
Potassium hydrooxide	0	0	0	0.001143
Argon	0.01477	0	0.007384	0
Melamine	7E-5	0	0	0
Isopropanol	0	1.99572	0	0
Bromine	0	0	0	0.001247
Ethanol	0	0	0	00.10281
Sulfuric acid	0	0	2.834E-5	0
Graphite	0	0	3.71E-10	0
Hydrogen peroxide	0	0	6.29E-9	0
Potassium permanganate	0	0	0.00020618	0
Glucose				0.003444
Chlorine	4.37E-7	0	3.226E-6	0
Electricity	1.6393	4.6621	4.5864	4.58571
Sum	1.6604	117.18662	4.59411	4.60682

Unit: kg 1,4-DCB .

Table S6 Life-cycle impact of terrestrial acidification.

Scenario	This work	Ref.1	Ref.2	Ref.3
Water deionised	2.84E-8	4.63E-6	5.79E-7	0
Carbon	5.84E-8	0	0	0
Nickel	33.8E-5	0.521	5.88E-6	6.29E-5
Iron(III)chloride	5.74E-8	0	1.29E-8	1.62E-7
Iron sulfate	0	1.14E-5	0	0
Potassium hydrooxide	0	0	0	3.94E-6
Argon	9.33E-5	0	4.66E-5	0
Melamine	4.73E-7	0	0	0
Isopropanol	0	0.012	0	0
Bromine	0	0	0	8.70E-6
Ethanol	0	0	0	7.07E-5
Sulfuric acid	0	0	7.44E-6	0
Graphite	0	0	1.58E-8	0
Hydrogen peroxide	0	0	1.53E-7	0
Potassium permanganate	0	0	6.89E-7	0
Glucose	0	0	0	1.18E-5
Chlorine	5.77E-8	0	9.15E-9	0
Electricity	0.00202	0.00575	0.005659	0.00565866
Sum	0.00216	0.539	0.005721	0.005817

Unit: kg SO_2 eq.

Table S7. Life-cycle impact of fine parcticulate matter formation

Scenario	This work	Ref.1	Ref.2	Ref.3
Water deionised	1.78E-8	2.89E-6	3.62E-7	0
Carbon	2.12E-8	0	0	0
Nickel	1.13E-5	00.16	1.75E-6	1.87E-5
Iron(III)chloride	3.04E-8	0	7.14E-9	9.02E-8
Iron sulfate	0	6.69E-6	0	0
Potassium hydrooxide	0	0	0	2.10E-6
Argon	6.1E-5	0	3.05E-5	0
Melamine	1.61E-7	0	0	0
Isopropanol	0	0.00453	0	0
Bromine	0	0	0	3.54E-6
Ethanol	0	0	0	4.11E-5
Sulfuric acid	0	0	2.20E-6	0
Graphite	0	0	7.10E-9	0
Hydrogen peroxide	0	0	7.35E-8	0
Potassium permanganate	0	0	3.63E-7	0
Glucose	0	0	0	3.81E-6
Chlorine	2.34E-8	0	3.72E-9	0
Electricity	0.000984	0.0028	0.0027502	0.00275
Sum	0.00106	0.168	0.0027855	0.00281909

Unit: kg PM2.5 eq.

Table S8. Life-cycle impact of ozone formation, human health

Scenario	This work	Ref.1	Ref.2	Ref.3
Water deionised	1.82E-8	2.97E-6	3.71E-7	0
Carbon	2.6E-8	0	0	0
Nickel	9.13E-7	0.033	1.41E-7	1.51E-6
Iron(III)chloride	3.33E-8	0	7.82E-9	9.88E-8
Iron sulfate	0	6.13E-6	0	0
Potassium hydrooxide	0	0	0	2.45E-6
Argon	5.81E-5	0	2.9E-5	0
Melamine	1.36E-7	0	0	0
Isopropanol	0	0.00818	0	0
Bromine	0	0	0	4.39E-6
Ethanol	0	0	0	6.57E-5
Sulfuric acid	0	0	3.29E-7	0
Graphite	0	0	1.58E-8	0
Hydrogen peroxide	0	0	8.96E-8	0
Potassium permanganate	0	0	4.68E-7	0
Glucose				5.18E-6
Chlorine	2.85E-8	0	4.52E-9	0
Electricity	0.00106	0.00301	0.0029596	0.002959
Sum	0.00112	0.0442	0.00299	0.0030386

Unit: kg NO_x eq.

Table S9. Life-cycle impact of fossil resource scarcity

Scenario	This work	Ref.1	Ref.2	Ref.3
Water deionised	1.94E-6	0.000316	3.94E-5	0
Carbon	2.88E-6	0	0	0
Nickel	3.92E-5	1.09	6.08E-6	6.50E--5
Iron(III)chloride	3.04E-6	0	7.16E-7	9.04E-6
Iron sulfate	0	0.000635	0	0
Potassium hydrooxide	0	0	0	0.000283
Argon	0.00677	0	0.003384	0
Melamine	3.33E-5	0	0	0
Isopropanol	0	2.57	0	0
Bromine	0	0	0	0.000907
Ethanol	0	0	0	0.0016762
Sulfuric acid	0	0	0.001891	0
Graphite	0	0	8.47E-7	0
Hydrogen peroxide	0	0	1.52E-5	0
Potassium permanganate	0	0	4.89E-5	0
Glucose	0	0	0	0.0047454
Chlorine	3.25E-6	0	5.15E-7	0
Electricity	0.105	0.297	0.29238	0.292346
Sum	0.111	3.96	0.298	0.295761

Unit: kg oil eq.

Table S10 Life-cycle impact of freshwater and marine eutrophication.

Scenario	This work	Ref 1	Ref 2	Ref 3
Water deionsed	1.0359E-10	4.722E-7	4.572E-7	2.162E-8
Iron chloride	7.132E-8	0	1.5769E-8	0
Iron sulfate	0	2.089E-6	0	1.475E-8
Nickel	1.16E-5	0.00076553	1.5253E-6	0
Nitric acid	0	1.1413E-5	0	0
Nickel sulfate	0	0	0	1.1446E-6
Melamine	5.261E-7	0	0	0
Hydrochloric acid	3.286E-8	0	4.794E-9	0
Carbon	0	0	1.4453E-7	0
Electricity	0.002059	0.0014862	0.004501	0.003217
Isopropanol	0	0.0004552	0	0
Argon	7.99E-6	0	3.164E-6	3.718E-5
Potassium hydroxide	0	0	0	7.348E-7
Bromine	0	0	0	8.612E-7
Acetic acid	0	0	0	6.361E-8
Acetone	0	0	0	5.158E-8
Sodium hydroxide	0	0	0	7.376E-8
Glucose	0	0	0	9E-6
Ethanol	0	0	0	0.0001781
sum	**0.00208**	**0.00272**	**0.00451**	**0.00345**

Unit: Kg P and N eq.

Table S11 EXAFS fitting parameters at the Fe K-edge for various samples（S_0^2=0.90 from Fe-foil）

	shell	CN[a]	R[b](Å)	σ^{2c}(Å^2)	ΔE_0[d](eV)	R factor
Fe-foil	Fe-Fe1	8*	2.45±0.01	0.0045	5.0±1.3	0.006
	Fe-Fe2	6*	2.84±0.01	0.0041		
Sample-Fe	Fe-Ni	10.81±1.5	2.59±0.07	0.0078	4.6±1.7	0.017
Fe_2O_3	Fe-O	6*	2.28±0.02	0.0043	1.2±0.9	0.008
	Fe-Fe	4*	3.34±0.02	0.0037		
FeO	Fe-O	6*	2.11±0.08	0.0150	3.2±0.7	0.004
	Fe-Fe	12*	3.06±0.04	0.0130		

[a]*CN*: coordination numbers; [b]*R*: bond distance; [c]σ^2: Debye-Waller factors; [d] ΔE_0: the inner potential correction. R factor: goodness of fit. Error bounds that characterize the structural parameters obtained by EXAFS spectroscopy were estimated as CN±20%; R ± 1%; σ^2 ± 20%.

Table S12. EXAFS fitting parameters at the Ni K-edge for various samples（S_0^2=0.70 from Ni-foil）

	shell	CN[a]	R[b](Å)	σ²[c](Å²)	ΔE₀[d](eV)	R factor
Ni-foil	Ni-Ni	12	2.47±0.01	0.0062	6.7±0.5	0.001
NiO	Ni-O	6	2.05±0.04	0.0080	3.7±1.0	0.005
	Ni-Ni	12	2.94±0.03	0.0073		
Ni-Sample	Ni-Ni	7.64±1.5	2.53±0.04	0.0062	-4.5±2.7	0.011
	Ni-Fe	3.94±0.7	2.57±0.09	0.0053		

[a]*CN*: coordination numbers; [b]*R*: bond distance; [c]σ^2: Debye-Waller factors; [d] ΔE_0: the inner potential correction. R factor: goodness of fit. Error bounds that characterize the structural parameters obtained by EXAFS spectroscopy were estimated as CN±20%; R ± 1%; σ^2 ± 20%.

Table S13 Concentrations of metal ions leached from the Ni_3Fe sample into the solution after 140 hours of continuous operation.

Elements	Concentration in Solution (ppm)
Fe	0.129
Ni	0.419

Table S14 The calculated Gibbs free energy for OER over Ni_3FeOOH at 0 V and 1.23 V.

Ni_3FeOOH	E_0	ZPE-TΔS	G_0	Pathway	G	G(U=0V)	G(U=1.23 V)	dG(U=1.233V)
*OH	-325.79	0.36	-325.43	$+2H_2O$	-353.87	0.00	0.00	0
*O	-320.24	0.07	-320.17	$+2H_2O+1/2H_2-e$	-352.01	1.86	0.63	0.63
*OOH	-329.34	0.39	-328.95	$+H_2O+H_2-e$	-349.97	3.90	1.44	**0.81**
*OO	-324.24	0.03	-324.21	$+H_2O+3/2H_2-e$	-348.63	5.24	1.55	0.11
Vo	-315.19	0.00	-315.19	$+H_2O+3/2H_2+O_2$	-349.52	4.35	0.66	-0.89

Table S15 The calculated Gibbs free energy for OER over NiOOH at 0 V and 1.23 V.

NiOOH	E_0	ZPE-TΔS	G_0	Pathway	G	G(U=0V)	G(U=1.233V)	dG(U=1.233V)
*OH	-307.28	0.36	-306.92	$+2H_2O$	-335.36	0.00	0.00	0
*O	-301.67	0.06	-301.61	$+2H_2O+1/2H_2-e$	-333.45	1.91	0.68	0.68
*OOH	-311.46	0.40	-311.07	$+H_2O+H_2-e$	-332.09	3.27	0.81	0.12
*OO	-305.15	0.03	-305.12	$+H_2O+3/2H_2-e$	-329.54	5.82	2.12	**1.31**
V_o	-296.57	0.00	-296.57	$+H_2O+3/2H_2+O_2$	-330.90	4.46	0.76	-1.36
*OH	-307.28	0.36	-306.92	$+2H_2+O_2-e$	-330.43	4.93	0.00	-0.76